

Anomalous Hall effect in ferromagnetic Weyl semimetal candidate $Zr_{1-x}V_xCo_{1.6}Sn$

Guangqiang Wang(王光强), Zhanghao Sun(孙彰昊), Xinyu Si(司鑫宇), Shuang Jia(贾爽)

Citation: Chin. Phys. B . 2020, 29(7): 077503 . **doi:** 10.1088/1674-1056/ab8da8
Journal homepage: http://cpb.iphy.ac.cn; http://iopscience.iop.org/cpb

What follows is a list of articles you may be interested in

Electrical transport and optical properties of Cd_3As_2 thin films

Yun-Kun Yang(杨运坤), Fa-Xian Xiu(修发贤), Feng-Qiu Wang(王枫秋), Jun Wang(王军), Yi Shi(施毅)

Chin. Phys. B . 2019, 28(10): 107502 . **doi:** 10.1088/1674-1056/ab3a91

Magnetoresistance hysteresis in topological Kondo insulator SmB_6 nanowire

Ling-Jian Kong(孔令剑), Yong Zhou(周勇), Hua-Ding Song(宋化鼎), Da-Peng Yu(俞大鹏), Zhi-Min Liao(廖志敏)

Chin. Phys. B . 2019, 28(10): 107501 . **doi:** 10.1088/1674-1056/ab3a89

Two-dimensional transport and strong spin-orbit interaction in $SrMnSb_2$

Jiwei Ling(凌霁玮), Yanwen Liu(刘彦闻), Zhao Jin(金昭), Sha Huang(黄沙), Weiyi Wang(王伟懿), Cheng Zhang(张成), Xiang Yuan(袁翔), Shanshan Liu(刘姗姗), Enze Zhang(张恩泽), Ce Huang(黄策), Raman Sankar, Fang-Cheng Chou, Zhengcai Xia(夏正才), Faxian Xiu(修发贤)

Chin. Phys. B . 2018, 27(1): 017504 . **doi:** 10.1088/1674-1056/27/1/017504

Total ionizing radiation-induced read bit-errors in toggle magnetoresistive random-access memory devices

Yan Cui(崔岩), Ling Yang(杨玲), Teng Gao(高腾), Bo Li(李博), Jia-Jun Luo(罗家俊)

Chin. Phys. B . 2017, 26(8): 087501 . **doi:** 10.1088/1674-1056/26/8/087501

Anomalous Hall effect in perpendicular CoFeB thin films

Zhu Tao

Chin. Phys. B . 2014, 23(4): 047504 . **doi:** 10.1088/1674-1056/23/4/047504

RAPID COMMUNICATION

Anomalous Hall effect in ferromagnetic Weyl semimetal candidate $Zr_{1-x}V_xCo_{1.6}Sn$*

Guangqiang Wang(王光强)[1], Zhanghao Sun(孙彰昊)[1], Xinyu Si(司鑫宇)[1], and Shuang Jia(贾爽)[1,2,3,4,†]

[1] *International Center for Quantum Materials, School of Physics, Peking University, Beijing* 100871, *China*
[2] *Collaborative Innovation Center of Quantum Matter, Beijing* 100871, *China*
[3] *CAS Center for Excellence in Topological Quantum Computation, University of Chinese Academy of Sciences, Beijing* 100190, *China*
[4] *Beijing Academy of Quantum Information Sciences, Beijing* 100193, *China*

(Received 12 March 2020; revised manuscript received 20 April 2020; accepted manuscript online 28 April 2020)

We grew single crystals of vanadium-substituted, ferromagnetic Weyl semimetal candidate $Zr_{1-x}V_xCo_{1.6}Sn$ from molten tin flux. These solid solutions all crystallize in a full Heusler structure ($L2_1$) while their Curie temperatures and magnetic moments are enhanced by V-substitution. Their resistivity gradually changes from bad-metal-like to semiconductor-like with increasing x while the anomalous Hall effect (AHE), which can be well fitted by Tian–Ye–Jin (TYJ) scaling,[1] is also enhanced. Moreover, we find an apparent electron–electron interaction (EEI) induced quantum correction in resistivity at low temperature. The anomalous Hall conductivity (AHC) dominated by the intrinsic term is not corrected.

Keywords: anomalous Hall effect, ferromagnetic Weyl semimetal, full Heusler, electron–electron interaction

PACS: 75.47.−m, 73.50.Jt, 72.80.Ga, 71.55.Ak **DOI:** 10.1088/1674-1056/ab8da8

1. Introduction

Discovery of Weyl semimetal has motivated the interest for investigating topological electronic structure and related transport properties of various semimetal materials.[2,3] Of particular interest is ferromagnetic (FM) semimetal in which the breaking of time reversal symmetry can generate large Berry-curvature-bearing Weyl nodes and strong intrinsic anomalous Hall effect (AHE) thereupon.[4] Very recently, the existence of Weyl quasi-particles and topological nontrivial surface states has been observed in FM semimetals $Co_3Sn_2S_2$ and Co_2MnGa in spectroscopic experiments.[5–7] These magnetic Weyl semimetals manifest a large, intrinsic AHE which is also believed to be a signature of the existence of topological Weyl nodes.[5,8] Understanding the mechanism of AHE and its correlation to the topological nontrivial band structure is crucial for the material design aiming for future electronic devices working based on the anomalous effect.

Heusler compounds represent a large family of materials crystallizing in closely related structures and many of them have been considered as the candidates of magnetic Weyl semimetal.[9,10] These candidates include half-Heusler GdPtBi and full-Heusler Co_2MnGa,[5,11] both of which exhibit large AHE. The Co-based full Heusler compounds have attracted much attention because they own some advantages such as strong magnetism and tunability which may promise their future applications in electronic devices. Their magnetic ground state is controlled by the interatomic distance and follows the well-known Slater–Pauling rule,[12–14] leading to a relatively high Curie temperature (T_C). Moreover, changing their crystalline symmetry can tune the AHE from null to very large while keeping the magnetization the same.[15] When the number of the valence electrons equals 26, the Co-based full Heusler compounds manifest a particular half-metallic Weyl semimetal state, i.e., the spin-up electron bands form a topological nodal line and Weyl nodes while the spin-down electron bands possess a fully opened gap.[15–17] These 26e compounds include $ZrCo_2Sn$, $TiCo_2Sn$, and VCo_2Ga, whose electronic structures have been well calculated.[16–18]

In this paper, we exam the magnetic and electric transport properties of single-crystalline vanadium-substituted $ZrCo_{1.6}Sn$. Previous studies on the poly-crystalline parents compounds, $ZrCo_2Sn$ and VCo_2Sn, reported their FM ground state.[19–22] Recent electronic structure calculations unveiled a pair of Weyl nodes 0.6 eV above the Fermi level for $ZrCo_2Sn$.[16] Moreover, the calculation also suggested that 10% of V-substitution on $TiCo_2Sn$ and 30% of Nb-substitution on $ZrCo_2Sn$ will shift the Fermi level to the Weyl nodes energy while keeping the main band topology unchanged.[16] However the AHE of the pristine and Nb-substituted $ZrCo_2Sn$ has not been analyzed thoroughly, although the single crystal growth, magnetic and electric transport properties have been reported.[23–25]

*Project supported by the National Natural Science Foundation of China (Grant Nos. 11774007 and U1832214), the National Key R&D Program of China (Grant No. 2018YFA0305601), and the Strategic Priority Research Program of the Chinese Academy of Sciences (Grant No. XDB28000000).

†Corresponding author. E-mail: gwljiashuang@pku.edu.cn

© 2020 Chinese Physical Society and IOP Publishing Ltd

Realizing the difficulty for growing single-crystalline $TiCo_2Sn$,[26,27] we successfully grew single crystals of $Zr_{1-x}V_xCo_{1.6}Sn$ with the $L2_1$ Heusler phase structure from molten tin flux. We found that their Curie temperature and magnetic moment are enhanced by V-substitution while the resistivity changes from bad-metal-like to semiconductor-like at $x = 0.35$. Their AHE, which can be well fitted by Tian–Ye–Jin (TYJ) scaling,[1] is also enhanced by V-substitution. Moreover, we find an apparent electron–electron-interaction (EEI) induced quantum correction in longitudinal resistivity at low temperature. On the other hand, the AHE, which is dominated by the intrinsic term, is not corrected.

2. Methods

Single crystals of $Zr_{1-x}V_xCo_{1.6}Sn$ were grown in tin-flux with zirconium powder (99.8%, Alfa Aesar), vanadium dendritic crystals (99.9%, GRINM), cobalt powder (99.8%, Alfa Aesar), and tin lumps (99.99%, GRINM) as starting materials with the molar Zr : V : Co : Sn ratio of $(1-x) : x : 2 : 19$. The mixture was placed in an alumina crucible and then sealed in a fused silica ampoule with 0.02 MPa argon gas. The ampoule was slowly heated to 1100 °C in furnace and kept at this temperature for 12 h, followed by a slow cooling to 1000 °C at a rate of 2 °C/h. At this temperature, large single crystals were separated from molten tin by centrifugal decanting. Every single crystal for electrical and magnetic measurement was polished. The thickness is about 0.1 mm or less and no residual tin was visible. With increasing V substitution, the crystals' shape evolves from a truncated octahedron to a well-faceted cube displaying large (100) faces [insets in Fig. 1(b)]. At the same time, the crystal size scales down with increasing x. For $x > 0.35$, the crystals are not large enough to be handled for electrical transport measurement and therefore we are limited for $x \leq 0.35$ in this study.

Power x-ray diffraction (Cu-$K\alpha$) measurements were conducted at room temperature with a Rigaku MiniFlex 600 diffractometer to confirm the crystal structure. The compositions of Zr, V, and Co for the series were determined by energy dispersive x-ray spectroscopy (EDS) in an X-Max 80. DC magnetization was measured by a Quantum Design superconducting quantum interference device magnetometer in a variety of applied fields ($\mu_0 H \leq 6$ T) and temperatures ($T = 2$–300 K). The samples were mounted and fixed by GE varnish on a brass stick, with fields perpendicular to the face of (100). AC electrical resistivity measurements were performed in a Quantum Design physical property measurement system ($T = 2$–300 K, -9 T $\leq \mu_0 H \leq 9$ T). A standard four-wire method was adopted using silver paste as the contacts. The resistivity and Hall effect measurements were conducted with fields normal to and currents within the (100) plane.

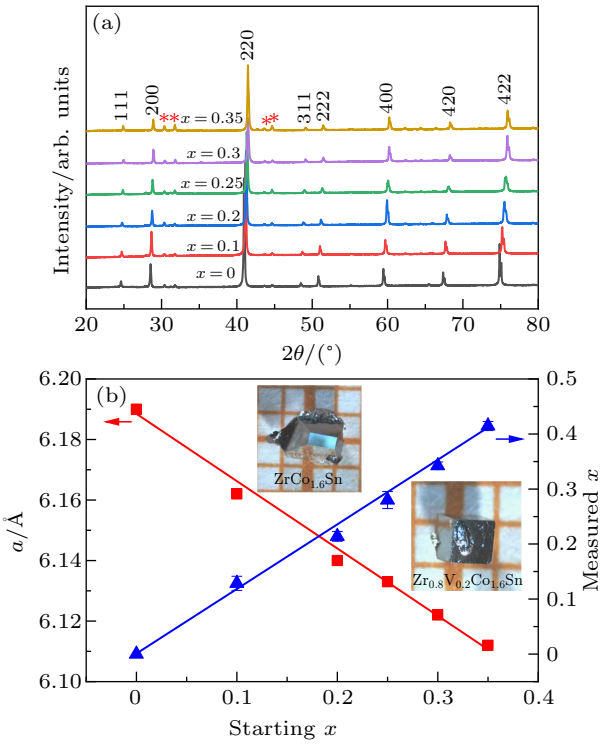


Fig. 1. (a) Power XRD results for all studied $Zr_{1-x}V_xCo_{1.6}Sn$ samples (asterisks mark the impurity peaks of tin flux). (b) The refined lattice constant a (red squares) and the measured vanadium concentration x by EDS against the starting x. Inset: Photos of two representative samples of $x = 0$ and 0.2.

3. Experimental results

Figure 1(a) shows the powder x-ray diffraction (XRD) patterns which match a standard Heusler $L2_1$ phase ($Fm\bar{3}m$) for all six samples $x = 0$, 0.1, 0.2, 0.25, 0.3, and 0.35. The peaks shift to higher angles as x increases, signifying a decreasing lattice constant. No unrelated phases were observed other than a few weak peaks of tin flux. The lattice constant, a, linearly drops with increasing x [Fig. 1(b)], which is consistent with the fact that V has smaller atomic radius than Zr. This linear lattice parameter change reflects a successful substitution of Zr atoms by V atoms which is also evidenced by EDS measurement. As shown in Fig. 1(b), the measured x from EDS and the starting x correspond well with each other within standard deviation. We notice that the lattice constant for the pristine sample is close to that of $ZrCo_{1.6}Sn$ reported in previous study.[23] This Co vacancy is the same as our EDS measurements on the Co composition for the whole series. Moreover, the saturated moment μ_{sat} and T_C are close to the reported values for $ZrCo_{1.6}Sn$ as well.[23] Therefore we determine that the whole series have about 20% Co vacancy and should be noted as $Zr_{1-x}V_xCo_{1.6}Sn$.

Figures 2(a) and 2(b) show temperature dependent magnetization under an applied magnetic field $\mu_0 H = 1$ T in a field-cooled (FC) mode and magnetic isotherms at 2 K for the whole series, respectively. The magnetization for all samples

shows a similar temperature dependence, signifying the transition from paramagnetic (PM) to FM state at around 200 K. The magnetic isotherms at 2 K show a typical profile of soft ferromagnet with a quickly saturated magnetic moment in an external field about 3 kOe. No obvious hysteresis loops can be discerned in any samples (data not shown here). It is noteworthy that the magnetization for $x = 0.35$ slightly increases at higher field, instead of being saturated like the other samples. Figure 2(c) summarizes the magnetic parameters including Curie–Weiss temperature θ_C, T_C, effective moment μ_{eff}, and μ_{sat} with respect to x. The θ_C and μ_{eff} are derived from the Curie–Weiss law fitting at high temperature while the T_C is determined by the magnetic isotherms near the T_C (Arrott's plot) (data not shown here). All the parameters are slightly enhanced by increasing x with the exception of $x = 0.35$, whose μ_{eff}, T_C, and θ_C are slightly smaller than those for $x = 0.30$. Previous studies on polycrystalline $Co_2Ti_{1-x}V_xSn$ suggested that the magnetic moment of Co does not linearly change with respect to x.[37,38] Instead, the Co moment reaches maximal when x is between 0.2 and 0.4. We infer the anomalous behavior for $x = 0.35$ is due to the fact that this sample is near the maximal point. Further study is needed for elaborating this unusual change.

Figure 2(d) shows the normalized temperature dependent resistivity $[\rho(T)/\rho(300\ \mathrm{K})]$ from 2 K to 300 K for all samples. All the $\rho(T)$ curves possess a negative temperature coefficient at high temperature and then they show a broad hump at around 200 K where the FM transition takes place. Below T_C, the samples of $x \leq 0.3$ have a bad-metal-like temperature dependent profile which is ended by an upturn at low temperature. With increasing x, the $\rho(T)$ curve gradually evolves from bad-metal-like below T_C to semiconductive at $x = 0.35$ for the whole temperature range. The low-temperature upturn becomes more evident and moves to higher temperature with increasing x, as denoted by the dotted line in Fig. 2(d). As shown below, the upturn is attributed to a quantum correction effect.

Figure 3 shows the Hall resistivity (ρ_{yx}) against external magnetic field for three representative samples at selected temperatures. They all display the same trend as the $M(H)$ curves at 2 K, signifying a strong AHE. The rapid saturated anomalous signal is followed by a normal Hall signal with a gentle, positive slope which reflects the dominating hole carrier. As temperature increases, the anomalous Hall signal weakens and finally fades away above T_C.

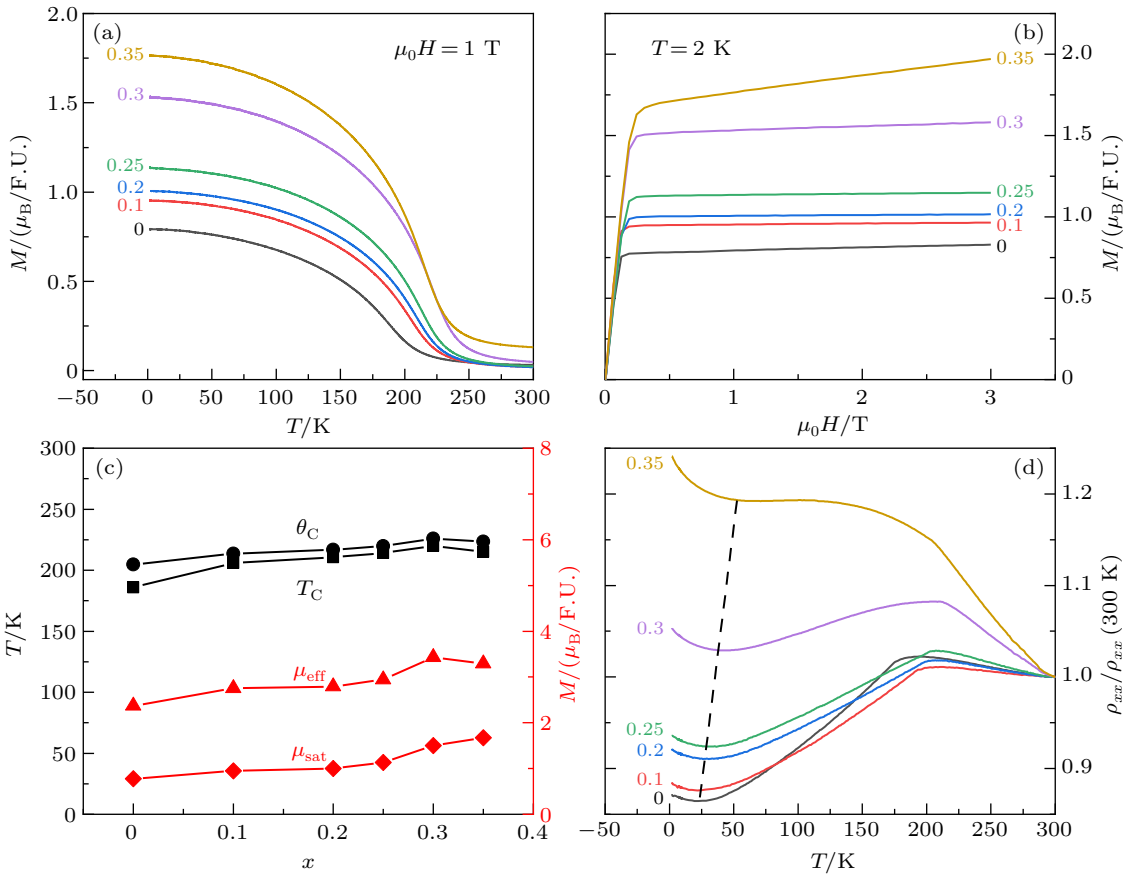


Fig. 2. (a) Temperature dependent magnetization of $Zr_{1-x}V_xCo_{1.6}Sn$ under an applied field of 1 T. (b) Field dependent magnetization at 2 K. (c) Curie–Weiss temperature θ_C, ferromagnetic Curie temperature T_C, effective moment μ_{eff}, and saturated moment μ_{sat} for different x. (d) The zero-field temperature variation of longitudinal resistivity for all samples. The dotted line connecting low temperature upturn points is a guide to the eyes.

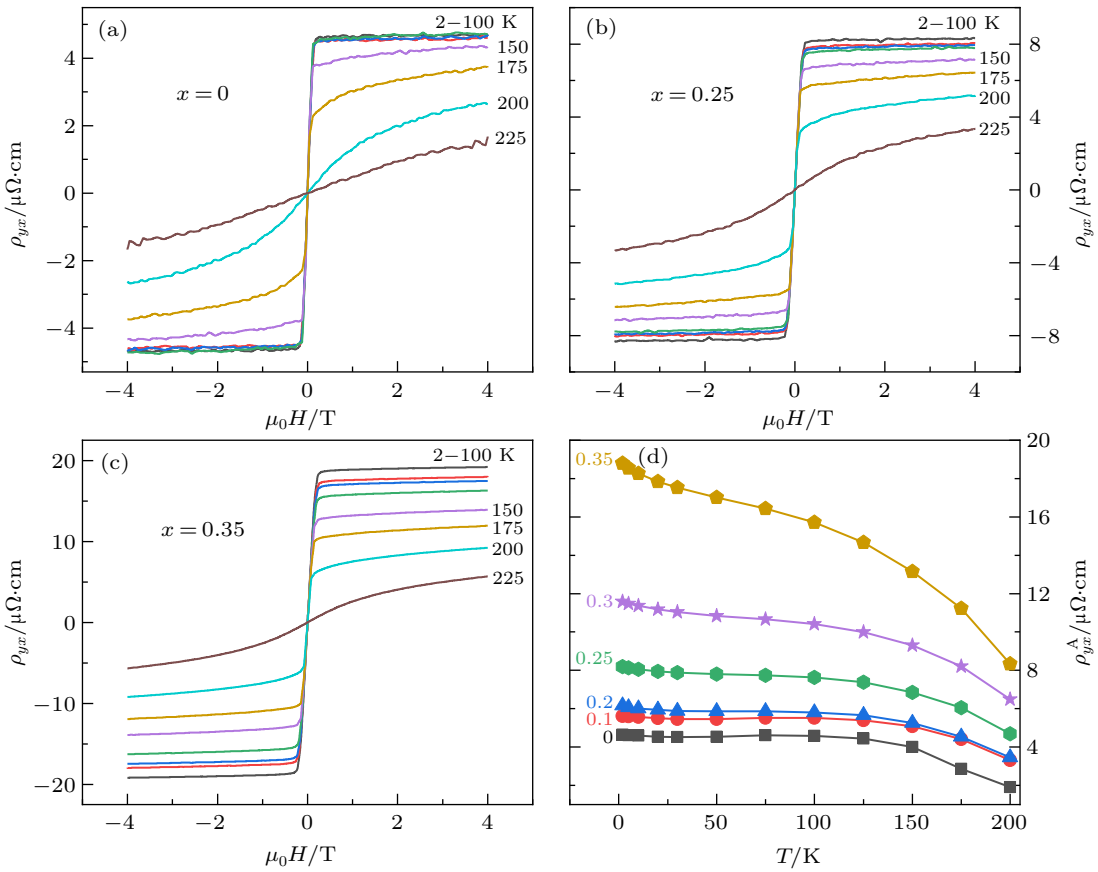


Fig. 3. (a)–(c) The Hall resistivity versus external field at selected temperatures for three representative samples $x = 0$, 0.25, and 0.35, respectively. (d) Temperature dependence of anomalous Hall resistivity for all series of samples.

Empirically, ρ_{yx} comprises two terms[28]

$$\rho_{yx} = \rho^{O}_{yx}(B) + \rho^{A}_{yx}(M) = R_0 B + \mu_0 R_S M, \tag{1}$$

where ρ^{O}_{yx} represents the ordinary Hall resistivity, ρ^{A}_{yx} the anomalous Hall resistivity, R_0 the ordinary Hall coefficient, and R_S the anomalous Hall coefficient. The anomalous Hall resistivity ρ^{A}_{yx}, obtained from the extrapolation of the high-field Hall resistivity to zero field, is shown against temperatures for all samples in Fig. 3(d). Apparently, $\rho^{A}_{yx}(T)$ does not simply reproduce the profile of $\rho(T)$ curve or $M(T)$ for any sample. This complicity indicates that the proper scale for the AHE in this system needs a comprehensive analysis of multiple effects.

4. Data analysis

In order to shed light on the mechanisms of AHE, the experimental data are fitted with the scaling laws in which the influence of $M(T)$ is also taken into account.[29–32] We find that the data can be well fitted by a modified TYJ scaling[1,33,34]

$$R_S = \rho^{A}_{yx}/\mu_0 M(T) = a'\rho_{xx0} + b\rho^{2}_{xx}, \tag{2}$$

where ρ_{xx0} is the residual resistivity induced by impurity scattering, $a'\rho_{xx0} = \alpha\rho_{xx0} + \beta\rho^{2}_{xx0}$ is the sum of the extrinsic contributions from skew scattering and side jump, and $b\rho^{2}_{xx}$ is the intrinsic contribution to R_S.

Figure 4 shows that R_S is linearly dependent on ρ^{2}_{xx} for all samples. For clarity, the data points above and below the low-temperature upturn are shown as solid and hollow symbols, respectively. These two segments lie almost on the same fitting line for one sample, signifying the validity of the TYJ scaling for a whole temperature range below T_C. The relatively large ρ_{xx0} (> 400 μΩ·cm) and small RRR (< 2) in $Zr_{1-x}V_xCo_{1.6}Sn$ imply that the impurity scattering prevails over phonon contribution. The validity of the TYJ scaling is consistent with the conclusion that the inelastic scattering from phonon plays a negligible role in skew scattering in comparison to the impurity scattering.[1,33,34]

The fitting coefficients a' and b, representing the extrinsic and intrinsic contributions, respectively, are plotted against x in Fig. 5(a). We notice that b remains positive for all x while a' shows sign reversal at $x = 0.25$. The reason of the sign change for the extrinsic AHC is unknown, but it may be related to the dominant contribution changing from side-jump to skew-scattering or vice versa. At this point, the two extrinsic terms can not be disentangled. The intrinsic AHC $\sigma^{int}_{AH} = \mu_0 M b$ and extrinsic AHC $\sigma^{ext}_{AH} = \frac{\mu_0 M a'}{\rho_{xx0}}$ at 2 K are shown as a function of x in Fig. 5(b). The intrinsic AHC doubles from 30 $\Omega^{-1}\cdot\mathrm{cm}^{-1}$ to

60 $\Omega^{-1}\cdot cm^{-1}$ with increasing x. These values are comparable to the calculated intrinsic AHC for 26*e* full Heusler VCo_2Ga and $TiCo_2Sn$.[10,18]

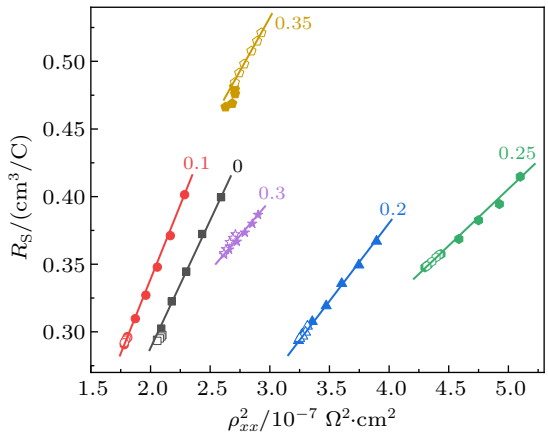


Fig. 4. The ρ_{xx}^2 dependence of R_S for each sample in which solid and hollow symbols denote the data above and below the low-temperature upturn, respectively. Solid lines are linear fit according to Eq. (2).

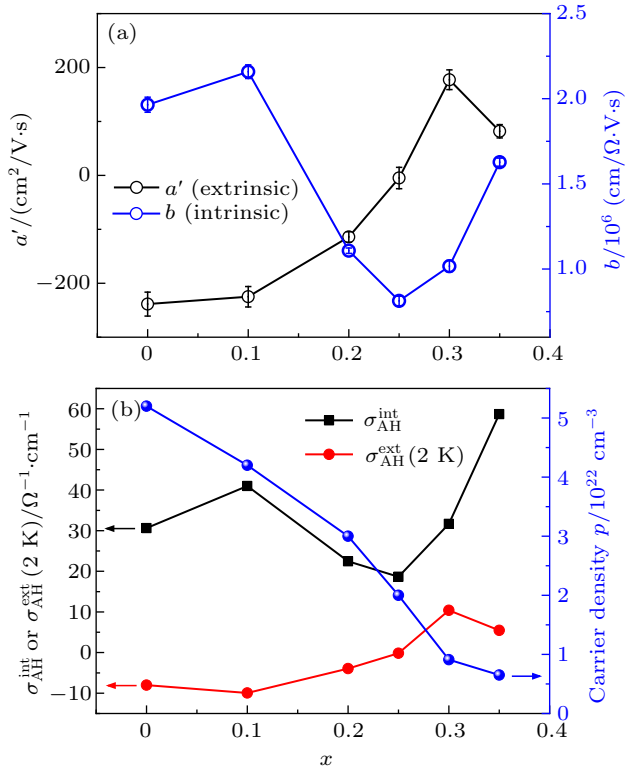


Fig. 5. (a) The fitting parameters a' and b as functions of the doping ratio x based on Eq. (2). (b) The variations of intrinsic AHC and extrinsic AHC at 2 K and carrier densities as x changes.

5. Discussion

We firstly discuss the crystalline and magnetic properties of $Zr_{1-x}V_xCo_{1.6}Sn$. As reported by Kushwaha *et al.*,[23] the tin-flux grown $ZrCo_2Sn$ crystals inevitably have Co vacancies which significantly suppress the T_C and μ_{sat}. The Co vacancies also affect the density of states of the minority spins in electronic structure.[35] Our measurements reveal that the properties of pristine $ZrCo_{1.6}Sn$ are close to those reported by Kushwaha *et al.*[23] and the whole series show the same Co vacancies. We also notice that the lattice parameters in polycrystalline $ZrCo_2Sn$ (6.25 Å) and VCo_2Sn (5.98 Å) differ in 0.27 Å,[21] which is approximately triple the change of a from $x = 0$ to 0.35. This linear change of a is consistent with our EDS measurements and verifies that Co vacancies are unchanged for different x.

Previous study showed that polycrystalline VCo_2Sn has $T_C = 105$ K and $\mu_{sat} = 1.2$ μ_B/F.U.[21] and therefore a naive expectation is that the magnetism will be suppressed by V-substitution in $ZrCo_{1.6}Sn$. In contrast, we observed that the T_C and μ_{sat} slightly increase until $x = 0.35$ in $Zr_{1-x}V_xCo_{1.6}Sn$, which conforms to the well-know Slater–Pauling rule[36] but contradicts the expectation. Please note this T_C change is also distinguished from the case of $Zr_{1-x}Nb_xCo_2Sn$[25] in which the Nb substitution leads to the weakening of ferromagnetism. This unexpected change of magnetization in our case is consistent with the previous studies on $Co_2Ti_{1-x}V_xSn$[37,38] in which the saturation magnetization initially increases with x until $x = 0.4$ and then drops. We speculate that it may be related to the chemical pressure difference while the 3d characteristics of V atoms may also play a role. Further elaboration on the whole series from $x = 0$ to 1 is needed for understanding this puzzle.

As theoretically predicted,[16] $ZrCo_2Sn$ has stable Weyl nodes located slightly above the Fermi level which can be tuned by alloying 30% Nb. Although the Co vacancies strongly modify the magnetic properties, the Weyl nodes should not be annihilated by the disorder as they are protected by the crystalline symmetry.[23] In $Zr_{1-x}V_xCo_{1.6}Sn$ we observed an enhanced intrinsic AHE which may be correlated with Weyl nodes energy approaching to the Fermi level. According to the previous calculation,[18] VCo_2Sn is not a half metal and it has an AHC as large as -1500 $\Omega^{-1}\cdot cm^{-1}$. However we do not observe a transition from positive to negative in the AHE for $Zr_{1-x}V_xCo_{1.6}Sn$ till $x = 0.35$. As shown in Fig. 5(b), the hole density (p) is gradually reduced with increasing V substitution until it reaches 5×10^{21} cm^{-3} for $x = 0.35$. This p-type behavior indicates that the chemical potential is not beyond the Weyl nodes energy yet. We expect that the AHC and carrier density will change significantly when $x > 0.35$.

In the last part, we clarify the low-temperature upturn in resistivity in Fig. 2(a) and the influence on the AHE. In general, the electron–electron Coulomb interaction (EEI) and weak localization (WL) are supposed to account for the resistivity upturn.[39–42] Their influence can be represented as

quantum corrections to the normal electron transport[43]

$$\rho_{xx}(T) = \rho_{xx0} + \rho_{\mathrm{EEI}}(T) + \rho_{\mathrm{WL}}(T), \tag{3}$$

where $\rho_{\mathrm{EEI}}(T)$ is proportional to $-T^{1/2}$ and $\rho_{\mathrm{WL}}(T)$ is proportional to $-T$ or $-T^{3/2}$ dependent on the dominant inelastic-scattering mechanism in three-dimensional systems.

Figure 6(a) shows a linear relation between $\Delta\rho(T) = \frac{\rho(T)-\rho(2\ \mathrm{K})}{\rho(2\ \mathrm{K})}$ and $T^{1/2}$ for all $Zr_{1-x}V_xCo_{1.6}Sn$ samples at low temperature, indicating that the upturn is mostly like to be the quantum correction from EEI. Figure 6(b) shows the normalized anomalous Hall coefficient $R_S/R_S(175\ \mathrm{K})$ plotted as a function of $T^{1/2}$. The R_S also displays an upturn dependence on $T^{1/2}$ at low temperatures. Figure 6(c) shows that the σ_{xy}^{A} has no obvious corrections from EEI for all $Zr_{1-x}V_xCo_{1.6}Sn$ samples.

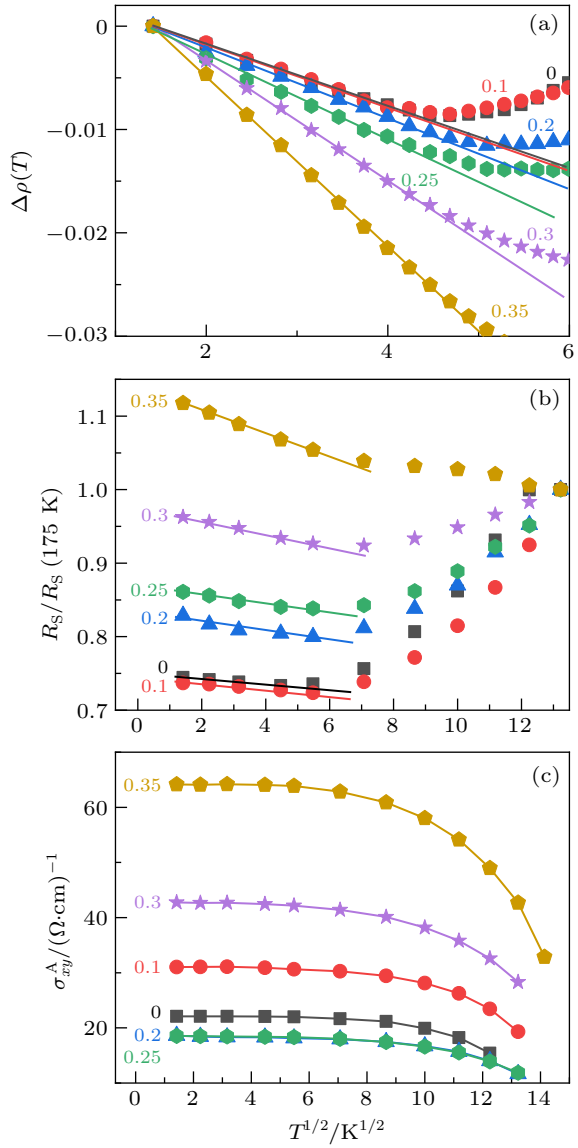


Fig. 6. The $T^{1/2}$ dependence of (a) normalized relative changes in longitudinal resistivities ρ_{xx} near and below the upturns, (b) normalized changes of anomalous Hall coefficients R_S and (c) anomalous Hall conductivities σ_{xy}^{A} for all studied samples.

It is well-known that the WL contributes to the extrinsic AHC[40,44] while the EEI will not lead to any correction to the AHC.[29,45,46] However recent experiment observed a large correction to the AHC originating from EEI in $HgCr_2Se_4$.[39] In contract, our measurements on $Zr_{1-x}V_xCo_{1.6}Sn$ show no correction to the AHC by EEI. Further study on various systems is needed for elaborating the relation between the quantum corrections and AHE.

6. Conclusion

In summary, we measured the magnetic and transport properties for FM Weyl semimetal candidate $Zr_{1-x}V_xCo_{1.6}Sn$ at $x \leq 0.35$. Their AHE can be well-fitted by the TYJ scaling law which yields a dominated intrinsic term. The intrinsic AHC is slightly enhanced by increasing x. It will be interesting to investigate the solid solutions with more V-substitution but different crystal growth technique is needed.

References

[1] Tian Y, Ye L and Jin X 2009 *Phys. Rev. Lett.* **103** 087206
[2] Armitage N P, Mele E J and Vishwanath A 2018 *Rev. Mod. Phys.* **90** 015001
[3] Zou J, He Z and Xu G 2019 *npj Comput. Mater.* **5** 96
[4] Burkov A A 2014 *Phys. Rev. Lett.* **113** 187202
[5] Belopolski I, Manna K, Sanchez D S, *et al.* 2019 *Science* **365** 1278
[6] Liu D F, Liang A J, Liu E K, Xu Q N, Li Y W, Chen C, Pei D, Shi W J, Mo S K, Dudin P, Kim T, Cacho C, Li G, Sun Y, Yang L X, Liu Z K, Parkin S S P, Felser C and Chen Y L 2019 *Science* **365** 1282
[7] Morali N, Batabyal R, Nag P K, Liu E, Xu Q, Sun Y, Yan B, Felser C, Avraham N and Beidenkopf H 2019 *Science* **365** 1286
[8] Liu E, Sun Y, Kumar N, *et al.* 2018 *Nat. Phys.* **14** 1125
[9] Wollmann L, Nayak A K, Parkin S S P and Felser C 2017 *Ann. Rev. Mater. Res.* **47** 247
[10] Manna K, Sun Y, Muechler L, Kübler J and Felser C 2018 *Nat. Rev. Mater.* **3** 244
[11] Suzuki T, Chisnell R, Devarakonda A, Liu Y T, Feng W, Xiao D, Lynn J W and Checkelsky J G 2016 *Nat. Phys.* **12** 1119
[12] Galanakis I, Dederichs P H and Papanikolaou N 2002 *Phys. Rev. B* **66** 174429
[13] Kübler J, Fecher G H and Felser C 2007 *Phys. Rev. B* **76** 024414
[14] Fechera G H, Kandpal H C, Wurmehl S and Felser C 2006 *J. Appl. Phys.* **99** 08J106
[15] Manna K, Muechler L, Kao T H, Stinshoff R, Zhang Y, Gooth J, Kumar N, Kreiner G, Koepernik K, Car R, Kübler J, Fecher G H, Shekhar C, Sun Y and Felser C 2018 *Phys. Rev. X* **8** 041045
[16] Wang Z, Vergniory M G, Kushwaha S, Hirschberger M, Chulkov E V, Ernst A, Ong N P, Cava R J and Bernevig B A 2016 *Phys. Rev. Lett.* **117** 236401
[17] Chang G, Xu S Y, Zheng H, Singh B, Hsu C H, Bian G, Alidoust N, Belopolski I, Sanchez D S, Zhang S, Lin H and Hasan M Z 2016 *Sci. Rep.* **6** 38839
[18] Kübler J and Felser C 2012 *Phys. Rev. B* **85** 012405
[19] Wolter A U B, Bosse A, Baabe D, Maksimov I, Mienert D, Klauß H H, Litterst F J, Niemeier D, Michalak R, Geibel C, Feyerherm R, Hendrikx R, Mydosh J A and Süllow S 2002 *Phys. Rev. B* **66** 174428
[20] Zhang W, Qian Z, Sui Y, Liu Y, Su W, Zhang M, Liu Z, Liu G and Wu G 2006 *J. Magn. Magn. Mater.* **299** 255
[21] Carbonari A W, Saxena R N, Pendl J W, Filho J M, Attili R N, Dionysio M O and de Souza S D 1996 *J. Magn. Magn. Mater.* **163** 313
[22] Yu T, Yu X, Yang E, Sun C, Zhang X and Lei M 2019 *Chin. Phys. B* **28** 067501
[23] Kushwaha S K, Stolze K, Wang Z, Hirschberger M, Lin J, Bernevig B A, Ong N P and Cava R J 2017 *J. Phys.: Condens. Matter* **29** 225702

[24] Kushwaha S K, Wang Z, Kong T and Cava R J 2018 *J. Phys.: Condens. Matter* **30** 075701
[25] Yang M, Gu G, Yi C, Yan D, Li Y and Shi Y 2019 *J. Phys.: Condens. Matter* **31** 275702
[26] Ernst B, Sahoo R, Sun Y, Nayak J, Müchler L, Nayak A K, Kumar N, Gayles J, Markou A, Fecher G H and Felser C 2019 *Phys. Rev. B* **100** 054445
[27] Hu J, Ernst B, Tu S, Kuveždić M, HamzićA, Tafra E, Basletić M, Zhang Y, Markou A, Felser C, Fert A, Zhao W, Ansermet J P and Yu H 2018 *Phys. Rev. Applied* **10** 044037
[28] Lee W L, Watauchi S, Miller V L, Cava R J and Ong N P 2004 *Science* **303** 1647
[29] Hazra B K, Kaul S N, Srinath S, Raja M M, Rawat R and Lakhani A 2017 *Phys. Rev. B* **96** 184434
[30] Zhu L J, Nie S H and Zhao J H 2016 *Phys. Rev. B* **93** 195112
[31] Ding J J, Wu S B, Yang X F and Zhu T 2015 *Chin. Phys. B* **24** 027201
[32] Zhu T 2014 *Chin. Phys. B* **23** 047504
[33] Hou D, Su G, Tian Y, Jin X, Yang S A and Niu Q 2015 *Phys. Rev. Lett.* **114** 217203
[34] Yue D and Jin X 2017 *J. Phys. Soc. Jpn.* **86** 011006
[35] Ślebarski A, Jezierski A, Neumann M and Plogmann S 1999 *Eur. Phys. J. B* **12** 519
[36] Graf T, Felser C and Parkin S S P 2011 *Prog. Solid State Chem.* **39** 1
[37] Dunlap R A and Stroink G 1982 *J. Appl. Phys.* **53** 8210
[38] Pendl J W, Saxena R N, Carbonari A W, Filho J M and Schaff J 1996 *J. Phys.: Condens. Matter* **8** 11317
[39] Yang S, Li Z, Lin C, Yi C, Shi Y, Culcer D and Li Y 2019 *Phys. Rev. Lett.* **123** 096601
[40] Mitra P, Misra R, Hebard A F, Muttalib K A and Wölfle P 2007 *Phys. Rev. Lett.* **99** 046804
[41] Shi G, Zhang M, Yan D, Feng H, Yang M, Shi Y and Li Y 2020 *Chin. Phys. Lett.* **4** 047301
[42] Wang Q, Yu P, Huang X, Fan J, Jing X, Ji Z, Liu Z, Liu G, Yang C and Lu L 2018 *Chin. Phys. Lett.* **35** 077303
[43] Lee P A and Ramakrishnan T V 1985 *Rev. Mod. Phys.* **57** 287
[44] Dugaev V K, Crépieux A and Bruno P 2001 *Phys. Rev. B* **64** 104411
[45] Langenfeld A and Wölfle P 1991 *Phys. Rev. Lett.* **67** 739
[46] Muttalib K A and Wölfle P 2007 *Phys. Rev. B* **76** 214415